JOURNAL OF GUIDANCE, CONTROL, AND DYNAMICS
Vol. 17, No. 6, November–December 1994

H_∞ Helicopter Flight Control Law Design With and Without Rotor State Feedback

Marc D. Takahashi*
NASA Ames Research Center, Moffett Field, California 94035-1000

An H_∞ formulation to design pitch-roll flight control laws for hovering helicopters is presented. Adjustment of the weight functions in the formulation is relatively straightforward. The feedback performance is set by the crossover frequency, which can be directly adjusted through the sensitivity $(I+KG)^{-1}$ weight function. The closed-loop stability is controlled by the complementary sensitivity $KG(I+KG)^{-1}$ weight function. The relative size of the dynamic gains is adjusted through the control $(I+KG)^{-1}K$ weight function. A framework to use the H_∞ compensation is also presented that allows systematic compliance to the quantitative low-speed requirements of a modern combat rotorcraft handling qualities specification (ADS-33C). Using this H_∞ formulation, control law designs were developed to investigate the effect of using rotor state feedback. Two laws were developed for an articulated rotor helicopter math model in low-speed flight: a compensator using rigid-body measurements and one using body plus rotor state measurements. Both laws were designed with similar crossover frequencies, stability margins, and response types. The design without rotor state feedback has the potential to pass approximately twice as much noise to the actuators near the 1/rev frequency as the design with rotor state feedback. Furthermore, the response of the controller without rotor state feedback was more sensitive to gain variations. Because of this sensitivity, the design without rotor state feedback, configured as a high-bandwidth rate response type, showed more high-frequency oscillation in roll.

Nomenclature

p, q, r	= fuselage roll, pitch, and yaw rate, deg/s
u, v, w	= longitudinal, lateral, and normal fuselage velocities, ft/s
u_g, v_g	= longitudinal and lateral gust disturbances, ft/s
$\beta_0, \beta_{1s}, \beta_{1c}$	= collective, sine, and cosine nonrotating flap degrees of freedom, deg
$\delta_A, \delta_E, \delta_P, \delta_C$	= lateral, longitudinal, pedal, and collective stick inputs, in.
$\delta_a, \delta_e, \delta_p, \delta_c$	= lateral, longitudinal, pedal, and collective inputs, %
$\zeta_0, \zeta_{1s}, \zeta_{1c}$	= collective, sine, and cosine nonrotating lead-lag degrees of freedom, deg
$\lambda_0, \lambda_{1s}, \lambda_{1c}$	= collective, sine, and cosine dynamic inflow degrees of freedom
ϕ, θ, ψ	= roll, pitch, and yaw fuselage attitudes, deg
ϕ_c^i, θ_c^i	= inner loop roll and pitch command

Introduction

FUTURE combat rotorcraft will require high levels of agility and maneuverability as well as capabilities for operating in degraded visual environments and adverse weather conditions.[1] High levels of feedback in the flight control system should make these performance requirements achievable by improving wind gust disturbance rejection and tracking performance. High-gain feedback, however, infringes into the frequency range of the coupled rotor-fuselage dynamics. These dynamics can cause problems in flight control design because of their high order and cross-axis coupling. These effects will become even more pronounced if newer technologies, such as bearingless rotors, are introduced into helicopter designs.

The problem herein is the design of multivariable, high-gain, feedback for the pitch-roll axes of helicopters with and without rotor state feedback. In the high-gain situation, the rotor is part of the dynamics that need to be controlled. Measurement of the rotor states gives the feedback direct access to the rotor dynamics and, therefore, can improve the quality of the feedback.[2,3] Multivariable methods are suited to the design of feedbacks for this type of problem, due to the high order and cross-axis coupling in the rotor-fuselage dynamics as well as the increased number of sensors associated with rotor state feedback. The objectives of this work are to develop a systematic design approach to apply a particular multivariable method, H_∞, and, further, to use this approach to assess differences between compensators with and without rotor state feedback. These objectives are met using analysis models that adequately represent the rotor-fuselage coupling and time delay in the system.

Multivariable methods fall into two broad categories, the first of which is eigenstructure methods,[4–8] where the designer assigns closed-loop eigenvalues and eigenvector elements. The second category is Riccati solution-based methods,[8–13] where the designer manipulates weight matrices (LQG, LQR) or frequency-dependent transfer function weight matrices (H_2 and H_∞) to control the compensator design. The H_∞ design method presented herein falls into the second category. A systematic design approach to adjust the weight matrices is presented, where the feedback performance is controlled by adjusting the crossover frequency through one weight function. Likewise, the closed-loop stability margins and the size of the dynamic gains are each controlled by other respective weight functions. Also presented is a method to apply this design approach to meet the quantitative low-speed requirements of the modern combat rotorcraft handling qualities specification ADS-33C.[1] Using this design approach, a comparison between feedback designs with and without rotor state feedback is then made. Two designs with and without rotor state feedback are discussed, where both have similar crossover frequencies, stability margins, and response types. These two comparable designs are then used to assess some differences between control laws with and without rotor state feedback.

Helicopter Analysis Models

The helicopter configuration used herein is a UH-60A Black Hawk, which is a four-bladed, articulated rotor, utility helicopter. Two distinct mathematical models are used to represent the UH-60 dynamics for linear and nonlinear analyses. The linear model was generated from the model described in Ref. 14, which represents the helicopter as a six-degree-of-freedom rigid fuselage with rigid rotor blades each with a flap and lag degree of freedom. No rpm degree-of-freedom and engine-governor dynamics are included in this model. Linear two-dimensional quasi-steady strip theory is used

Received Sept. 3, 1993; revision received May 2, 1994; accepted for publication May 3, 1994.

*Aerospace Engineer, Aeroflightdynamics Directorate, U.S. Army Aviation and Troop Command. Member AIAA.

to model the rotor blade aerodynamic forces, and a three-state Pitt-Peters dynamic inflow model is used to capture the unsteady wake effects.

The linearized design model has 23 perturbation states, of which 8 define the body motion (p, q, r, u, v, w, ϕ, and θ) and 12 nonrotating frame states define the flap and lag motions of the rotor ($\beta_0, \dot{\beta}_{1s}, \dot{\beta}_{1c}, \zeta_0, \dot{\zeta}_{1s}, \dot{\zeta}_{1c}, \beta_0, \beta_{1s}, \beta_{1c}, \zeta_0, \zeta_{1s}$, and ζ_{1c}). The dynamic inflow model is defined by the states λ_0, λ_{1s}, and λ_{1c}. The design flight condition is in hover at a gross weight of 16,800 lb at standard sea-level air density with the rotor speed fixed at 27 rad/s.

Time responses of the control design were generated using the nonlinear UH-60 simulation program discussed in Ref. 15. This model has a blade element rotor model with flap and lag degrees of freedom and was modified to include the three-state Pitt-Peters inflow model. Static look-up tables provide blade aerodynamic, rotor downwash, and fuselage aerodynamic forces. The rotor rpm degree of freedom and the component-level T700 engine with rpm governor are also modeled as well as the nonlinear actuators, mixing box, and lead-lag damper systems.

Control System Framework and Design Approach

The control framework and aircraft dynamics are shown in Fig. 1. The aircraft dynamics in Fig. 1a includes the UH-60 dynamics and two sets of actuator dynamics, which are second-order systems. The two sets of actuators represent the fly-by-wire driver actuators and UH-60 primary actuators, which contribute approximately 10 and 20 ms of delay, respectively. Assuming a 50-Hz sample rate, the total delay from the zero-order hold (ZOH) and the computational delay is near 20 ms.

The sensor and antialiasing filter delays are lumped together and represent approximately 50 ms of time delay, giving a total loop delay near 100 ms. In the nonlinear model, a multiblade coordinate transformation was applied to the blade rotating positions and rates in order to transform them to the nonrotating motions. The nonrotating motions and the body motions were then passed through third-order Bessel filters to give the rotor and body measurements used herein. The blade measurements used herein are an approximation, since measuring the rotor motions would require a device such as a kinematic observer,[16] which would produce filtered rotating blade flap positions and rates before the multiblade coordinate transformation was applied. Modeling the sensors to this level of complexity, however, was felt to be beyond what was needed to meet the objectives of this paper.

The general control framework is shown in Fig. 1b. The control loops are broken into two sets of axes, pitch-roll and yaw-heave. Breaking the problem into these two sets is a natural simplification. Most of the complex dynamic coupling occurs between the pitch and roll axes through the rotor sine and cosine degrees of freedom and the fuselage roll and pitch degrees of freedom. The yaw and heave axes couple with the rotor collective degrees of freedom and the fuselage yaw and rpm-engine-governor degrees of freedom.

This structure was chosen to make the process of achieving compliance with ADS-33C more systematic by taking advantage of some properties of the helicopter dynamics and the quantitative hover specifications in ADS-33C. Broadly speaking, most of these requirements can be met by response shaping, which does not affect the feedback properties of the control law. Only two types of requirements in the specification need to be addressed by the feedback: the disturbance rejection requirements and the pole placement requirements. The pole placement requirements concern the lateral and longitudinal phugoid modes, which dominate the translational motions of the helicopter. The disturbance rejection requirements are determined by the crossover behavior, which affects the higher frequency pitch-roll attitude modes. For typical helicopters, the frequency separation between the translational and attitude modes is

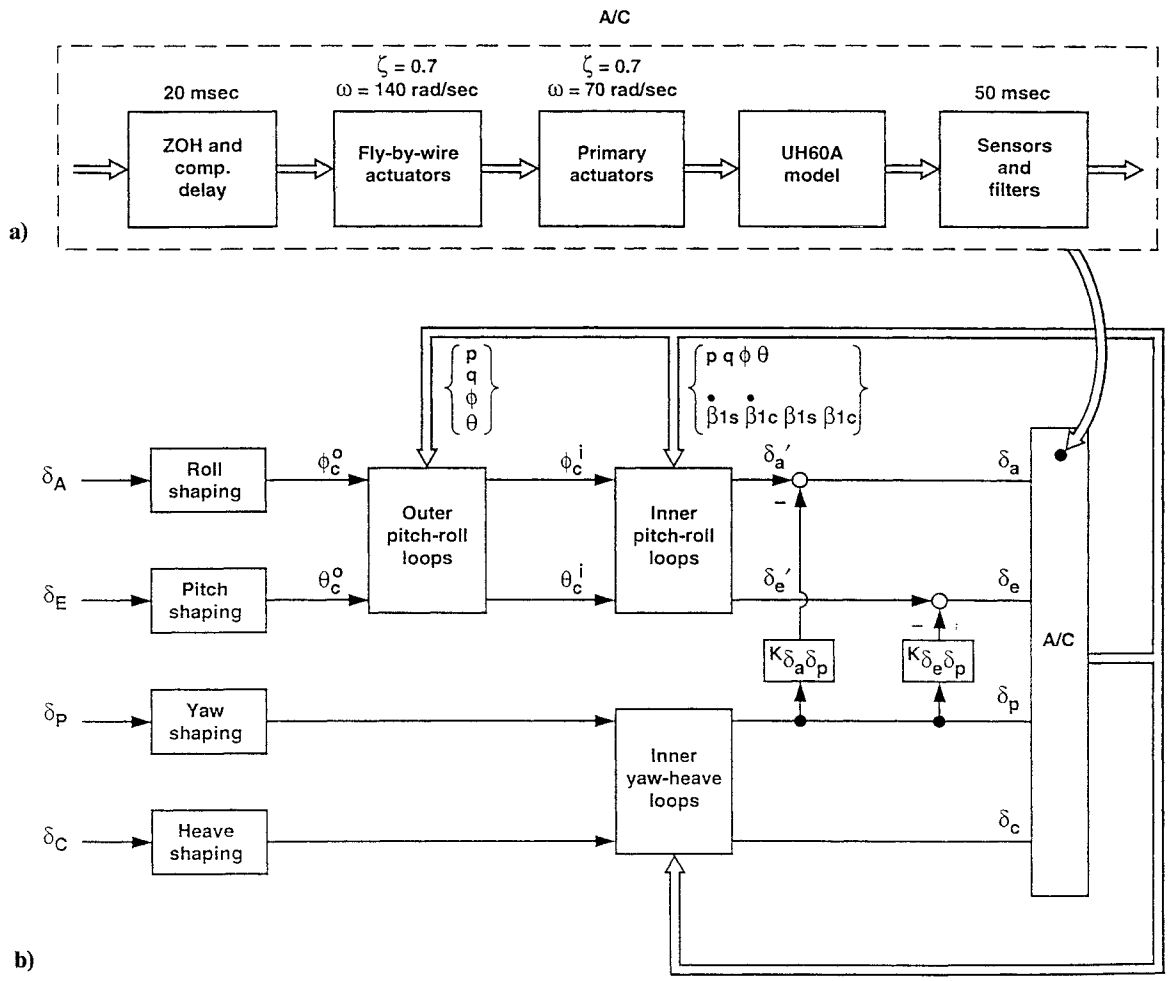

Fig. 1 Control system structure.

large, but it is not so large that the two sets of modes can be handled independently. Separation of these modes is large enough, however, that they can be handled sequentially.

The inner pitch-roll loops are closed first and are used to manage the high-frequency crossover behavior. These loops are high gain and they dominate the disturbance rejection properties of the feedback near the crossover frequency, and it is in these loops where the H_∞ design method is applied. The disturbance rejection will be achieved without resorting to integrators within the inner loops, which makes the body attitude measurements essential. The ADS-33C disturbance rejection criteria in pitch and roll require the crossover frequencies to be at least 2 and 3.5 rad/s, respectively. However, it should be noted that the crossover behavior also determines the robustness of the feedback with respect to model uncertainty. Although no such robustness requirements are explicitly written in ADS-33C, there is an implicit assumption that the performance should be maintained for all flight conditions. Therefore, a high level of feedback was set, 5 rad/s crossover, and a requirement was imposed to have at least 45 deg of phase margin and 6 dB of gain margin.

The outer pitch-roll loops are closed next and are used to meet the low-frequency pole placement requirements on the lateral and longitudinal phugoid modes. These loops are low gain with crossover frequencies on the order of 20% or less of the inner loop crossover frequencies. Because of this low gain, the outer loop closures do not greatly affect the crossover characteristics previously set by the inner loops. The system with only the inner loops closed will wash out attitude. Additional integrators are included in the outer loop to prevent this attitude washout and give the system an attitude-hold capability. Once the inner and outer pitch-roll loops are closed, the system response type is attitude-command, attitude-hold. The final responses in these axes are then modified through on-axis response shaping to give either attitude rate or attitude command responses.

Just as with the inner pitch-roll loops, the yaw-heave loops are used to set the disturbance rejection properties for these axes. The yaw-heave loops were designed as separate single-input, single-output loops using first-order approximations to the dynamics in these axes. In yaw, the crossover frequency was set at 4 rad/s, which meet the ADS-33C yaw gust disturbance rejection requirements, whereas in heave the crossover was set near 2 rad/s. Phase margins were 55 and 70 deg and gain margins were 10 and 16 dB for the yaw and heave axes, respectively. A constant crossfeed between the collective and pedal controls was also necessary to remove some of the coupling between the two axes.

Complete separation of the pitch-roll axes from the yaw-heave axes does not truly exist, since there is coupling primarily from the cant of the tail rotor and its offset from the center of roll of the helicopter. The $K_{\delta_a\delta_p}$ and $K_{\delta_e\delta_p}$ gains in the figure simply counteract the expected tail rotor moments. The respective gains were set to a constant approximation of the ratios of transfer functions $(p/\delta_p)/(p/\delta_a)$ and $(q/\delta_p)/(q/\delta_e)$.

H_∞ Formulation

The H_∞ problem herein is one of finding a stabilizing compensator K that satisfies

$$\|T_{11}\|_\infty < \gamma \tag{1}$$

The function T_{11} is the u_1-to-y_1 transfer function matrix of the closed-loop system shown in Fig. 2. The transfer function matrix P is typically defined as in Refs. 8, 12, and 13. However, the following alternate form was chosen, which will facilitate the design process:

$$\begin{pmatrix} y_1 \\ y_2 \end{pmatrix} = \left[\begin{array}{ccc|c} W_S & 0 & 0 & I \\ \hline GW_S & -W_R & -GW_T & G \end{array}\right] \begin{pmatrix} u_1 \\ u_2 \end{pmatrix} = [P] \begin{pmatrix} u_1 \\ u_2 \end{pmatrix} \tag{2}$$

Assuming this form, the closed-loop response from u_1 to y_1 is

$$y_1 = [\, SW_S \;\; RW_R \;\; TW_T \,]u_1 = [T_{11}]u_1 \tag{3}$$

The transfer function matrices W_S, W_R, and W_T are the frequency-dependent weight matrices and are used to control the shape of the sensitivity matrix $S = (I + KG)^{-1}$, the control input matrix

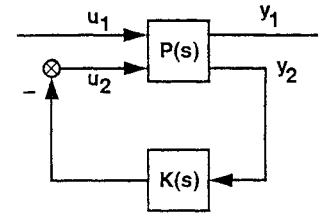

Fig. 2 Basic block diagram.

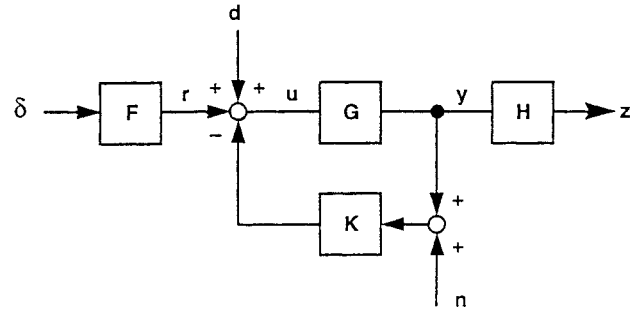

Fig. 3 Block diagram of noise and disturbance.

$R = (I + KG)^{-1}K$, and the complementary sensitivity matrix $T = (I + KG)^{-1}KG$, respectively. These matrices will be used to determine the closed-loop properties of the system.

The matrices R and T determine the closed-loop robustness to the additive unstructured uncertainty model and the multiplicative unstructured uncertainty model at the plant input.[17] The role of S and R is seen in the relationship of noise and disturbances to the actuator and the tracking error responses given by

$$\begin{pmatrix} u \\ e \end{pmatrix} = \begin{bmatrix} S & -R \\ -HGS & HGR \end{bmatrix} \begin{pmatrix} d \\ n \end{pmatrix} \tag{4}$$

This relationship is based on Fig. 3, which shows the noise n, disturbances d, outputs z, and inputs u of the closed-loop system. The tracking error $e = \delta - z$ is the difference between the commanded response δ and the corresponding subset of outputs z. The matrix H has zero or unity elements to only pass the roll and pitch attitudes to the output. The quantity HG, which appears in the second row of Eq. (4), is a given and cannot be altered by the feedback K. Therefore, the two fundamental transfer function matrices in Eq. (4) are S and R. The matrix S determines how disturbances pass to the actuator and the tracking error responses, whereas R determines how the noise passes to these responses.

Inner Pitch-Roll Design

The inner loop is the model-following structure shown in Fig. 4. Starting from the left, the first block contains the approximate inverse of the roll and pitch open-loop responses and the unshaped responses (M). The unshaped responses are necessary for this block to be realizable and were chosen to give a second-order attitude response type for both axes ($\omega = \sqrt{2}$ and $\zeta = 0.8$). Pitch-roll decoupling is also contained within this block. The next block is an approximate model of the coupled pitch and roll open-loop dynamics. The compensator K is designed using the H_∞ method and measurements shown from the aircraft are those for the case with rotor state feedback.

The design model on which the inner loop compensator is based is a 14-state reduced model of the 23-state linear model. The states retained were $p, q, \phi, \theta, \dot{\beta}_{1s}, \dot{\beta}_{1c}, \dot{\zeta}_{1s}, \dot{\zeta}_{1c}, \beta_{1s}, \beta_{1c}, \zeta_{1s}, \zeta_{1c}, \lambda_{1s}$, and λ_{1c}, whereas the inputs retained were the lateral input δ_a and the longitudinal input δ_e. For the case with body measurements, the outputs are p, q, ϕ, and θ, whereas, for the case with body and rotor measurements, the outputs are $p, q, \phi, \theta, \dot{\beta}_{1s}, \dot{\beta}_{1c}, \beta_{1s}$, and β_{1c}. The velocity states u and v were removed, since they are dominated by the lateral and longitudinal phugoid modes, which have significantly lower frequencies than where the crossover frequency will be set. The states $r, w, \dot{\beta}_0, \dot{\zeta}_0, \beta_0, \zeta_0$, and λ_0 are related to the yaw-heave

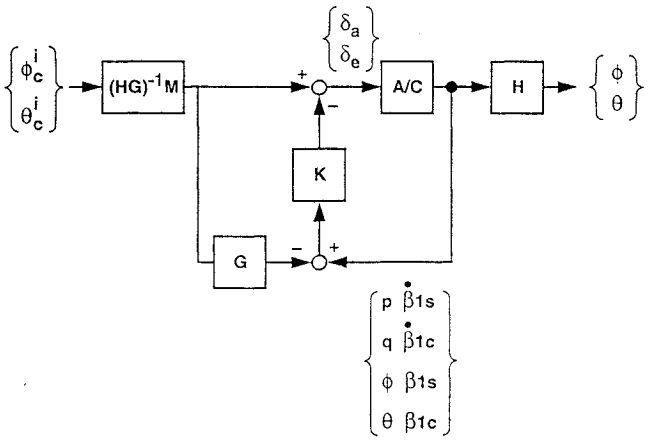

Fig. 4 Pitch-roll inner loop structure.

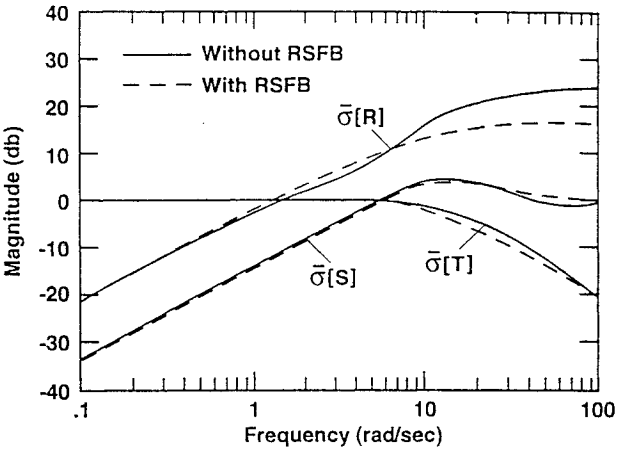

Fig. 5 Pitch-roll singular values with and without rotor state feedback.

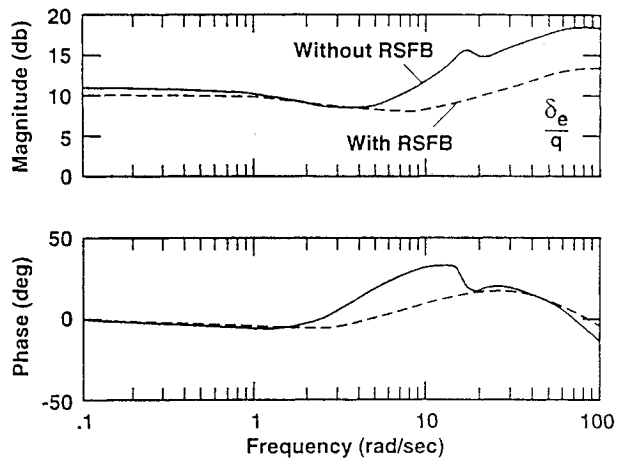

Fig. 6 δ_e from q gain with and without rotor state feedback.

dynamics and were removed. The approximate 100 ms of loop delay was also appended to the design model at the inputs.

The compensator was calculated using matrix operations on the state-space form of Eq. (2) The solution to satisfy Eq. (1) can be found by using the two-Riccati-solution method in Ref. 18. The augmentation of the system with the various weight transfer function matrices and the design model both produce compensation that is larger than the design model. However, reductions of the compensation back to 14 states were possible using frequency-weighted balanced realizations.

The weight matrices W_S, W_T, and W_R are diagonal with the ith diagonal elements defined by

$$w_S^i = \frac{b_{S0}^i}{s+0.01}, \qquad i = \delta_a, \delta_e \tag{5}$$

$$w_T^i = \frac{s/b_{T1}^i}{0.001s+1}, \qquad i = \delta_a, \delta_e \tag{6}$$

$$w_R^i = \frac{b_{R1}^i s + b_{R0}^i}{s+0.01}, \qquad i = p, q, \phi, \theta, \dot{\beta}_{1s}, \dot{\beta}_{1c}, \beta_{1s}, \beta_{1c} \tag{7}$$

The 2×2 matrix W_S has approximate roll-pitch integrator elements with crossover frequencies at b_{S0}^i. The 2×2 matrix W_T has approximate roll-pitch differentiator elements with crossover frequencies at b_{T1}^i. The W_R matrix is 4×4 for the design without rotor state measurements or it is 8×8 for the design with rotor state measurements. Each element is an approximate integrator-plus-proportional element associated with p, q, ϕ, and θ for the design without rotor state measurements or $p, q, \phi, \theta, \dot{\beta}_{1s}, \dot{\beta}_{1c}, \beta_{1s}$, and β_{1c} for the design with rotor state measurements. The approximate integrator gain is controlled by b_{R0}^i, whereas b_{R1}^i controls the gain of the approximate proportional element. The precise values in the weight functions can be found in Ref. 19 along with all of the other values that define the control laws described in this paper.

The weight W_S was set first with W_R set to a small value. The function of W_S is to control the performance of the feedback through the low-frequency shape of $\bar{\sigma}[S]$. By the choice of weight functions, the matrix T_{11} in Eq. (3) is dominated by SW_S below the crossover frequency. If γ is set near unity, the compensator solution, by Eq. (1), will be such that the maximum singular value of T_{11} will be less than unity. As W_T is increased, SW_S will force $\|T_{11}\|_\infty$ against the unity boundary in the low frequency. Since W_S is nearly an integrator, S will have to take the form of a differentiator with a crossover near the value of the W_S function.

After choosing W_S, the weight W_T was adjusted to control the multiplicative stability robustness via the high-frequency shape of $\bar{\sigma}[T]$. By the choice of weight functions, T_{11} in Eq. (3) is dominated by TW_T above the crossover frequency. If γ is set near unity, the compensator solution, by Eq. (1), will be such that the maximum singular value of T_{11} will be less than unity. As W_T is increased, TW_T forces $\|T_{11}\|_\infty$ against the unity boundary in the high frequency. Since W_T is a differentiator, T will have to take the form of an integrator above the crossover frequency of W_T. Therefore, to control the robustness, the crossover frequency of W_T is decreased (i.e., the size of W_T is increased) to reduce $\bar{\sigma}[T]$ in the high frequency. The smaller $\bar{\sigma}[T]$ can be made, the better is the closed-loop robustness.

The weight W_R was adjusted last and was used to control the size of the dynamic gains, thus affecting the noise properties and additive robustness properties of the feedback. The high-frequency part of the gains can be adjusted by using the proportional part of W_R. In the high frequency, S tends to the identity and the proportional part of W_R dominates the W_R matrix. By definition, $R = SK$, so, in the high frequency, the proportional part of W_R is a weight on K. The low-frequency part of the individual gains can be adjusted by using the integral part of W_R. In the low frequency, S tends toward a differentiator and the integral part of W_R dominates the W_R matrix. Again, by definition, $R = SK$, so, in the low frequency, the integral part of W_R is a weight on K. As the integral part of W_R is increased, the gains are reduced and, consequently, $\bar{\sigma}[R]$ is reduced in the low frequency. There is limit on how high the integral part of W_R can be raised, since the gains must still be sufficient to achieve the desired level of performance. The integral part of the weight function is critical in preventing integrators from appearing in the dynamic gains. The relative size of each element of W_R determines the relative size of the gains to each other. Thus, increasing the weight on the p measurement relative to the weight on the ϕ measurement reduced the gains $K_{\delta_a p}$ and $K_{\delta_e p}$ relative to $K_{\delta_a \phi}$ and $K_{\delta_e \phi}$.

Using the weight functions in this manner, compensators were designed with 5 rad/s crossover frequencies for the cases with and without rotor state feedback. The singular values for both cases are shown in Fig. 5. Both cases were purposely designed with similar S and T shapes, so they would have similar performance and stability robustness. The case without rotor state feedback (RSFB), however, has a much larger $\bar{\sigma}[R]$ than the case with rotor state feedback. By Eq. (4), one can expect nearly twice as much sensor noise will pass

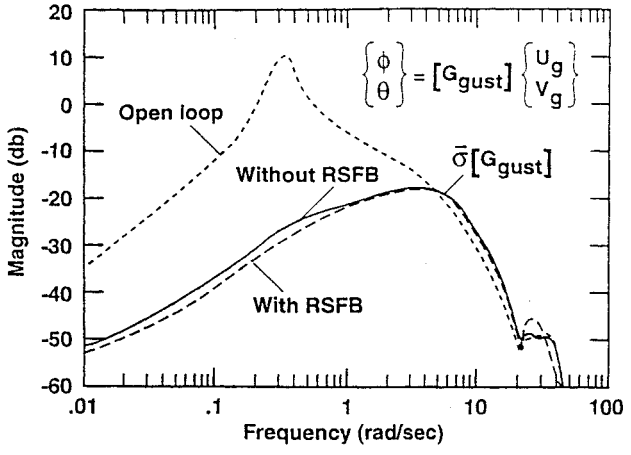

Fig. 7 Open- and closed-loop disturbance rejection.

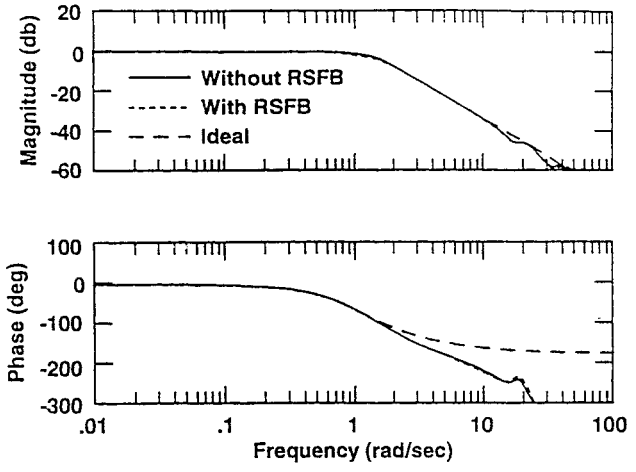

Fig. 8 Unshaped roll axis closed-loop responses.

through the system at the 1/rev frequency (i.e. the rotor speed). It should be noted that this is a worst-case situation since the measure used to make this assessment is the largest singular value. A more precise value for the gain limits using the two designs would be desirable; however, such a limit is not possible without far more accurate modeling of the sensors, sensor noise, blade flexibility effects, and rotor aerodynamic effects. Without rotor state feedback, the control law K must introduce lead to overcome the effective time delay of the rotor to attain the same level of performance as the case with rotor state feedback. This extra lead will cause the feedback to pass extra noise, which is reflected as the increase in $\bar{\sigma}[R]$. The lead can also be seen in the gains, as shown Fig. 6, which compares the δ_e-from-q gain for the cases with and without rotor state feedback.

Outer Pitch-Roll Loops

When the inner loops are closed, both the pitch and roll axes wash out attitude due to the translation modes of the system. The function of the outer loops is to remove this washout in attitudes using small gains relative to the inner loop gains. Each axis was managed as a single-loop proportional-integral-derivative (PID) design problem. With the inner loops closed, both the ϕ/ϕ_c^i and θ/θ_c^i transfer functions are approximately those of a second-order system. The feedbacks from p, ϕ, and $\int \phi$ for the roll axis and feedbacks from q, θ, and $\int \theta$ for the pitch axis were then chosen to form a PID feedback whose numerator canceled the second-order system. This choice of gains yielded approximate 1/s behavior, whose crossover frequency was set to 0.8 rad/s. This crossover was high enough to remove the velocity washout effects but is only 16% of the inner loop crossover frequency. Because of the 1/s behavior, the outer loop crossover frequency is also the approximate closed-loop pole location. ADS-33C requires at least 0.35 damping in the lateral and longitudinal modes, so the real-valued pole set by the crossover was sufficient to meet the pole placement requirement.

Feedback and Response Characteristics

The return ratios of the roll and pitch axes were each inspected with all other loops closed, and both showed an effective 1/s magnitude behavior near the crossover frequency. Without rotor state feedback, the roll axis had a crossover frequency at 5.4 rad/s with 50 deg of phase margin and 7.4 dB of gain margin. The pitch axis had a 5.1-rad/s crossover frequency with 55 deg of phase margin and 8.1 dB of gain margin. With rotor state feedback, the roll axis had a crossover frequency at 5.6 rad/s with 49 deg of phase margin and 7.4 dB of gain margin. The pitch axis had a 5.5-rad/s crossover frequency with 54 deg of phase margin and 8.4 dB of gain margin. The similar margin is the result of designing the two laws with essentially the same stability robustness properties and shows the level of control over feedback properties in using this design approach.

The closed-loop stability of the two control systems away from the hover design point was checked using several off-design linear models. These models were generated by varying the flight speed (15 knots backward; 1, 15, 30, and 45 knots forward; 15 knots right; 15 knots left), the air density (sea level and 5000 ft), and the gross weight (14,000, 16,800, and 20,000 lb). Both closed-loop systems remained stable throughout all of the flight conditions.

Disturbance rejection of the closed-loop system is shown in the $\bar{\sigma}[G_{gust}]$ plot in Fig. 7. The disturbances are pure longitudinal and lateral translational gusts. Both designs have very similar disturbance rejection properties, achieving nearly 30 dB of attenuation in the low frequency. Most of the disturbance rejection is due to the inner loop feedback, with the outer loops contributing more at low frequencies. Also seen in the figure is the slight amplification of disturbances occurring above the crossover frequencies, which is a natural consequence of this feedback.

The response characteristics were achieved through prefiltering. The pitch and roll axes were set to either rate or attitude command response types by approximately canceling the closed-loop, on-axis response and replacing it with the desired response. Figure 8 shows the unshaped, closed-loop, on-axis roll response ($\omega_\phi = \sqrt{2}$ and $\zeta_\phi = 0.8$). The responses with and without rotor state feedback are shown along with the ideal response. No attempt was made to cancel the time delay that is inherent in the unshaped response, so the prefilters only have the second-order response characteristics in their numerator. The desired responses were chosen to comply with the on-axis response requirements in ADS-33C. Two response types were chosen: a rate command (for aggressive maneuvering) and an attitude command (for all other mission task elements). For the roll attitude response, the shaping took the form

$$\frac{s^2 + 2\omega_\phi \zeta_\phi s + \omega_\phi^2}{s^2 + 2\omega_d \zeta_d s + \omega_d^2} \tag{8}$$

whereas for a rate response the form was

$$\frac{T_d s + 1}{s} \frac{s^2 + 2\omega_\phi \zeta_\phi s + \omega_\phi^2}{s^2 + 2\omega_d \zeta_d s + \omega_d^2} \tag{9}$$

where the subscript d indicates the desired response characteristics. The pitch axis was managed in the same fashion. Also included in the on-axis shaping was a stick sensitivity and stick rate limiting.

Several time responses of the closed-loop nonlinear system to moderate stick inputs were generated to check compliance to ADS-33C attitude quickness requirements. The responses of the pitch and roll attitudes were adequately decoupled (less than 15%), and control motion responses did not exceed actuator position or rate limits for both of the designs with and without rotor state feedback. Figure 9 shows the roll response of the design with rotor state feedback configured as an attitude command response type to a doublet input. Twenty degrees of roll attitude is achieved with reasonable control motions. The responses with and without rotor state feedback are virtually indistinguishable for this response type.

Although the responses for the attitude command response type were virtually indistinguishable, the design without rotor state feedback is, in fact, more sensitive to variations away from the design point than the system with rotor state feedback. This sensitivity can

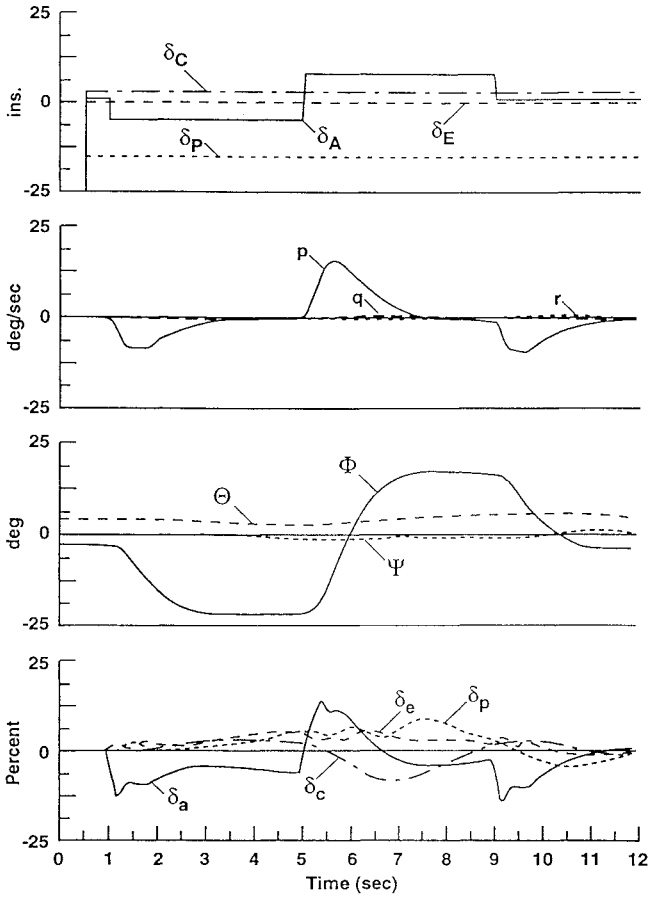

Fig. 9 Roll response of attitude command response with rotor state feedback.

be seen more clearly using the more aggressive rate command response type. Figure 10 shows angular rate responses to a lateral doublet input at four different gain factors with and without rotor state feedback. The gain factor increases the roll loop gain, so a gain factor of 2.0 doubles the design crossover frequency from 5 to 10 rad/s. The responses for both systems are quite different. As the gain is increased, a 2-Hz oscillation shows up in the responses without rotor state feedback far more forcefully than in the responses without rotor state feedback. This figure shows the crossover frequency of the design with rotor state feedback will have to be raised much higher from the nominal 5 rad/s, more than 50%, before this 2-Hz oscillation shows itself with the same effect as the design without rotor state feedback. Likewise, the crossover frequency of the case without rotor state feedback will have to be halved before the 2-Hz oscillation is diminished to the level as appears in the design with rotor state feedback.

The 2-Hz oscillation can be explained by considering the constant-gain feedback discussed in Ref. 3. It was shown that the rotor-fuselage coupling produces pitch- and roll-rate dynamics that are each closer to second-order, rather than to first-order dynamics. The latter are the classical dynamics if one assumes no rotor and fuselage coupling. A limitation in controlling the closed-loop flapping-plus-body modes occurs using only constant-gain body state feedback, since these measurements access only part of the rotor-fuselage dynamics. The additional use of rotor-flapping feedback gives access to all of these second-order dynamics, allowing more control over the closed-loop flap plus fuselage modes. This second-order behavior was particularly strong in the roll axis and was associated with the flap-regressing mode. The complex pair of poles associated with this mode tended to go unstable near 1 Hz (with 100 ms of time delay) using only constant body-attitude and body-rate feedback. This characteristic was true regardless of the ratio of roll-rate to roll-attitude gain. Adding constant flap sine feedback allowed complete access to the second-order dynamics, so one could cancel the flap-regressing poles giving 1/s like feedback. Increasing gain, in this case, produces poles that migrate toward

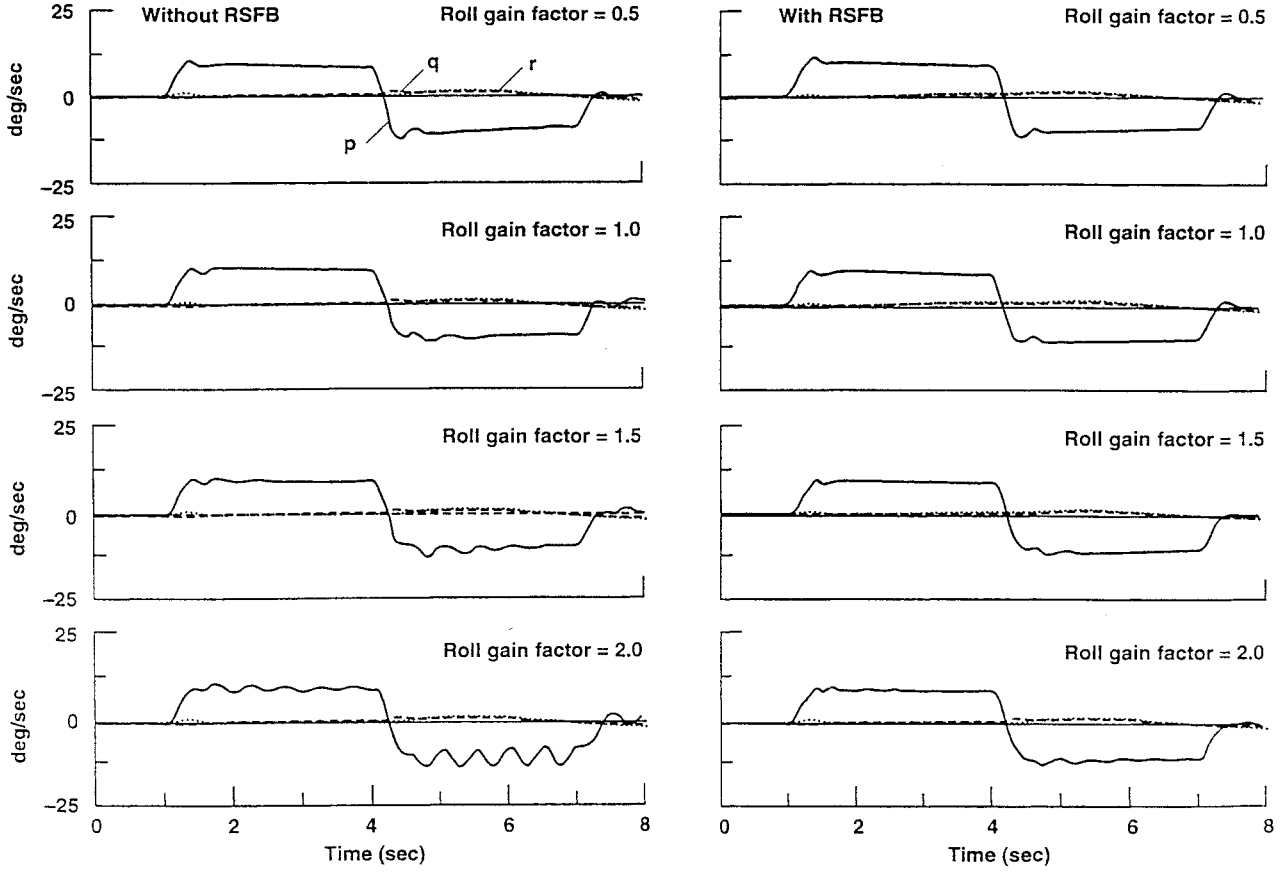

Fig. 10 Effect of increasing roll bandwidth on angular rate responses with and without rotor state feedback.

the right-half of the s plane nearer to 2 Hz. The dynamic compensation with rotor state feedback herein cancels the regressing flap poles in a similar fashion. Without rotor state feedback, the flap dynamics must be reconstructed, but the penalty for this is a loss of robustness as compared to actually measuring the flapping dynamics.

Conclusions

An H_∞ design method was formulated for the design of helicopter pitch-roll feedback. A control law framework for using the H_∞ design method was also presented that facilitated compliance to the quantitative low-speed requirements of the modern combat rotorcraft handling qualities specification ADS-33C. The method was applied to an articulated rotor helicopter configuration in low-speed flight. A design with only rigid-body measurements and a design with body and rotor state measurements were considered. Both laws were designed with similar 5-rad/s crossover performance, stability margins, and response types. The design without rotor state feedback was shown to have the potential to pass approximately twice as much noise to the actuators near the 1/rev frequency as the case with rotor state feedback. The control law without rotor state feedback was more sensitive to gain variations. When configured as an aggressive roll-rate response type, a 2-Hz oscillation appeared in the system without rotor state feedback far more forcefully than in the system with rotor state feedback.

References

[1]Aeronautical Design Standard-33C, Handling Qualities Requirements for Military Rotorcraft, U.S. Army Aviation Systems Command, St. Louis, MO, Aug. 1989.

[2]Chen, R. T. N., "An Exploratory Investigation of the Flight Dynamic Effects of Rotor rpm Variations and Rotor State Feedback in Hover," 18th European Rotorcraft Forum, Avignon, France, Sept. 1992.

[3]Takahashi, M. D., "Flight Control Design Using Rotor-State Feedback for an Articulated Rotor Helicopter in Hover," NASA TM-103967 or USAATCOM TR-92-A-012, Jan. 1993.

[4]Ekblad, M., "Synthesis of a Reduced Order Model and Design of a Multivariable Flight Control System for a High Performance Helicopter," AIAA/AHS/ASEE Aircraft Design, System Operations Meeting Paper A88-51972, Atlanta, GA, Sept. 1988.

[5]Garrard, W. L., Low, E., and Prouty, S., "Design of an Attitude and Rate Command Systems for Helicopters Using Eigenstructure Assignment," *Journal of Guidance, Control, and Dynamics*, Vol. 12, No. 6, 1989, pp. 783–791.

[6]Manness, M. A., and Murray-Smith, D. J., "Aspects of Multivariable Flight Control Law Design for Helicopters Using Eigenstructure Assignment," *Journal of the American Helicopter Society*, Vol. 37, No. 3, 1992, pp. 18–32.

[7]Suikat, R., "A Translational-Rate Command Control Law for Hover Assist," paper presented at 18th European Rotorcraft Forum, Avignon, France, Sept. 1992.

[8]Ingle, S. J., and Celi, R., "Effects of Higher Order Dynamics on Helicopter Flight Control Law Design," paper presented at 48th Annual Forum of the American Helicopter Society, Washington, DC, June 1992.

[9]Hall, W. E., and Bryson, A. E., "Inclusion of Rotor Dynamics in Controller Design for Helicopters," *Journal of Aircraft*, Vol. 10, No. 4, 1973, pp. 200–206.

[10]Miyajima, K., "Analytical Design of a High Performance Stability and Control Augmentation System for a Hingeless Rotor Helicopter," *Journal of the American Helicopter Society*, July 1979, pp. 29–36.

[11]Holdridge, R. D., Hindson, W. S., and Bryson, A. E., "LQG-Design and Flight Test of a Velocity Command System for a Helicopter," AIAA Guidance and Control Conference, Snowmass, CO, 1985.

[12]Yue, A., and Postlethwaite, I., "H_∞ Design and the Improvement of Helicopter Handling Qualities," 13th European Rotorcraft Forum, Arles, France, Sept. 1987.

[13]Takahashi, M. D., "Synthesis and Evaluation of an H_2 Control Law for a Hovering Helicopter," *Journal of Guidance, Control, and Dynamics*, Vol. 16, No. 3, 1993, pp. 579–584.

[14]Takahashi, M. D., "A Flight-Dynamic Helicopter Mathematical Model with a Single Flap-Lag-Torsion Main Rotor," USAAVSCOM TM 90-A-004 or NASA TM-102267, Feb. 1990.

[15]Ballin, M. G., and Dalang-Secretan, M. A., "Validation of the Dynamic Response of a Blade-Element UH-60 Simulation Model in Hovering Flight," 46th Annual Forum of the American Helicopter Society, Washington DC, 1990.

[16]McKillip, R. Jr., "Experimental Studies in System Identification of Helicopter Rotor Dynamics," *Vertica*, Vol. 12, No. 4, 1988, pp. 329–336.

[17]Maciejowski, J. M., *Multivariable Feedback Design*, Addison-Wesley, Wokingham, England, UK, 1989.

[18]Doyle, J. C., Glover, K., Khargonekar, and Francis, B. A., "State-Space Solutions to Standard H_2 and H_∞ Control Problems," *IEEE Transactions on Automatic Control*, Vol. 34, No. 8, 1989, pp. 831–847.

[19]Takahashi, M. D., "Design and Comparison of Pitch-Roll H_∞ Control Laws with and Without Rotor-State Feedback for a Hovering Helicopter," NASA TM-108793 or USAATCOM TR 93-A-013, Jan. 1994.